Programmable RNA *N*6-methyladenosine editing by CRISPR-Cas9 conjugates

Xiao-Min Liu[1], **Jun Zhou**[1,2], **Yuanhui Mao**[1], **Quanquan Ji**[1], **Shu-Bing Qian**[1,*]
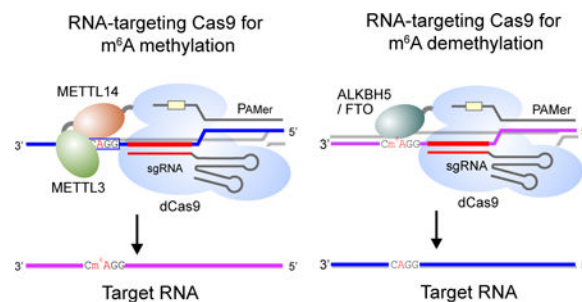
[1]Division of Nutritional Sciences, Cornell University, Ithaca, NY 14853, USA

[2]Present address: School of Life Science and Technology, China Pharmaceutical University, Nanjing 211198, China

Abstract

RNA modification in the form of N^6-methyladenosine (m^{6}A) regulates nearly all the post-transcriptional processes. The asymmetric m^{6}A deposition suggests that regional methylation may have distinct functional consequences. However, current RNA biology tools do not distinguish the contribution of individual m^{6}A modifications. Here we report the development of "m^{6}A editing", a powerful approach that enables m^{6}A installation and erasure from cellular RNAs without changing the primary sequence. We engineered fusions of CRISPR-Cas9 and a single chain m^{6}A methyltransferase that can be programmed with a guide RNA. The resultant m^{6}A "writers" allow functional comparison of single site methylation in different mRNA regions. We further engineered m^{6}A "erasers" by fusing CRISPR-Cas9 with ALKBH5 or FTO to achieve site-specific demethylation of RNAs. The development of programmable m^{6}A editing not only expands the scope of RNA engineering, but also facilitates mechanistic understanding of epitranscriptome.

Graphical Abstract

Reporting Summary

Further information on research design is available in the Nature Research Reporting Summary linked to this article.

Introduction

Reversible RNA modification forms the epitranscriptomic code that regulates gene expression beyond the primary sequence [1,2]. In eukaryotic cells, the most abundant internal RNA modification is N^6-methyladenosine (m^{6}A). Recognizing the core consensus sequence RR<u>A</u>CH (R, purine; H, non-guanine base), the responsible m^{6}A methyltransferase exists as a functional complex consisting of METTL3, METTL14, and WTAP [3–5]. The discovery of FTO and ALKBH5 in the demethylation pathway suggests the dynamic feature of m^{6}A modification [6,7]. The m^{6}A mark is decoded by specific "readers" to mediate a variety of downstream effects on RNA metabolism [8,9]. A recent study further reported that m^{6}A repels certain RNA-binding proteins [10], forming an additional layer in controlling dynamic RNA-protein interaction. Despite the tremendous progress in the functional characterization of m^{6}A modification, the regional effects of mRNA methylation remain obscure. The transcriptome-wide m^{6}A mapping revealed an asymmetric distribution of mRNA methylation with the majority of methylation clustered near the stop codon [11,12]. Recent m^{6}A-seq studies also revealed m^{6}A peaks in 5'UTR and start codons when plotting the peak density along the transcriptome. However, current RNA biology tools do not distinguish the contributions of individual m^{6}A modifications, imposing a significant barrier to our understanding of the mechanism by which m^{6}A markers influence cellular activities.

Recent advances in CRISPR-based technologies have revolutionized biomedical research by enabling precision genome editing [13–15]. From targeted DNA cleavage/repair to direct base editing, genetic components can be engineered with high efficiency and specificity. Gene expression is also subjected to regulation by DNA methylation and histone modifications (the 'epigenome') [16,17]. By fusing catalytically dead Cas9 (dCas9) to DNA or histone modifying enzymes, site-specific epigenome engineering becomes possible [18,19]. With the availability of Cas proteins capable of targeting single-stranded RNA [20,21], programmable editing of epitranscriptome by coupling RNA-targeting Cas with RNA base-modifying enzymes would be attractive. However, such implementation is held back by several challenges. First, our knowledge about the RNA modification machinery remains rudimentary. Second, a direct sequencing method for quantitative profiling of site-specific RNA base modifications is still lacking. Third, the complex physiological effect of RNA modifications hinders functional interpretation of engineered epitranscriptome. In the case of m^{6}A modification, it is unclear whether particular outcomes require a single RNA methylation event or an ensemble of m^{6}A modifications that function as a synergistic unit.

Here we report the development of "m^{6}A editing", a powerful approach that enables m^{6}A installation and erasure from cellular RNAs without changing the primary sequence. We created engineered m^{6}A "writers" by fusing CRISPR-Cas9 and a single chain m^{6}A methyltransferase. We further engineered m^{6}A "erasers" by fusing CRISPR-Cas9 with full length ALKBH5 or FTO to achieve site-specific demethylation of RNAs. The resultant m^{6}A

editors can be programmed with a guide RNA, allowing functional comparison of single site methylation in different mRNA regions.

Results

Designing programmable m⁶A writers.

Much of our knowledge of m⁶A is built upon genetic perturbations of modifying enzymes, which have pleiotropic effects on cellular physiology. It also inevitably affects global RNA methylation. To interrogate the regional effect of m⁶A, current methods often rely on point mutations that permanently remove the modification site from the transcript of interest. However, the altered nucleotide sequence may introduce unwanted properties and complicate data interpretation. It is thus highly desirable to develop a method that can manipulate individual m⁶A modifications at specific sites of individual transcripts without changing the primary sequence. We attempted to engineer the m⁶A machinery into a programmable RNA base modifier by taking advantage of RNA-guided dCas9 [20,21]. m⁶A is installed on RNA molecules by a MTase complex comprising METTL3, METTL14, and WTAP via recognition of the consensus sequence RRACH (R, purine; H, non-guanine base) [8,9]. Structural studies revealed that METTL3 primarily functions as the catalytic core, while METTL14 serves as an RNA-binding platform [22,23]. Since the METTL3-METTL14 heterodimer possesses strong catalytic activity, we constructed a single-chain m⁶A MTase by linking two MTase domains derived from human METTL3 and METTL14 respectively (Fig. 1a). We expressed and purified two fusion proteins with different orientations of MTase domains. *In vitro* methyltransferase assay showed that M3M14 exhibited >3 fold higher catalytic activity than M14M3 (Supplementary Fig. 1a). Consistent with the previous finding that AdoMet binds to the DPPW motif of METTL3 [22,23], introducing D395A mutation abolished the catalytic activity of both recombinant proteins (Supplementary Fig. 1a).

We next fused M3M14 to the amino terminus of dCas9 using the same linker designed for the DNA base editor (Supplementary Fig. 1b) [24]. Unlike the endogenous METTL3 or METTL14, which are primarily localized in the nucleus, both M3M14-dCas9 and M3^D395AM14-dCas9 fusion proteins showed predominant cytosolic localization in transfected HEK293T and MEF cells (Supplementary Fig. 1c and 1d). Although physiological m⁶A modification occurs on nascent RNAs in a co-transcriptional manner [25], the cytosolic presence of engineered m⁶A "writers" offers an attractive approach to targeting mature RNAs for *de novo* methylation. Similar to DNA-targeting dCas9, RNA-targeting dCas9 requires sequence-specific guide RNA (sgRNA) and the protospacer adjacent motif (PAM) supplied by an antisense oligonucleotide (PAMer) (Fig. 1a). Consistent with the previous report [20], we found that PAMer is essential for efficient binding of M3M14-dCas9 to the target RNA (Supplementary Fig. 2a). With two regional base pairing conferred by sgRNA and PAMer, possible off-targeting of dCas9 can be minimized, thereby increasing the specificity of RNA targeting.

Programmable 5'UTR m⁶A modification.

To assess whether M3M14-dCas9 is capable of inducing site-specific m⁶A modification, we first designed sgRNAs targeting the 5'UTR of Hsp70 mRNA. Since the level of endogenous

Hspa1a is undetectable in MEF cells under the normal growth condition, we introduced a firefly luciferase (Fluc) reporter bearing the 5'UTR of *Hspa1a* (Fig. 1b). In transfected MEF cells, the exogenous 5'UTR exhibited basal m^6A modification at A103 as evidenced by RT-qPCR of methylated RNA fragments enriched by m^6A antibodies (m^6A-RIP). This modification represents a genuine m^6A mark because it is highly sensitive to METTL3 knockdown (Supplementary Fig. 2b). To test whether M3M14-dCas9 can further boost the m^6A signal at this position, we designed a panel of four sgRNAs with their 5' ends located at varied distances to A103 (Fig. 1b). Overexpression of M3M14-dCas9 alone had negligible effect on total RNA methylation (Supplementary Fig. 2c). However, Co-transfection of sgRNA and PAMer resulted in site-specific m^6A modification at A103 of *Hspa1a*-Fluc with varied efficiencies (Fig. 1b). We observed a >50% increase of m^6A signals for sgRNA(b) and sgRNA(c), suggesting an effective window of ~10 nt for targeted methylation. This is consistent with the flexible nature of the XTEN linker between M3M14 and dCas9. The increased methylation was due to the catalytic activity of the engineered m^6A "writer" because little methylation was observed upon expression of M3^{D395A}M14-dCas9. The induced m^6A modification was site-specific because a putative m^6A site at the coding region of Fluc (A1280) showed comparable methylation signals regardless of the sgRNA presented (Fig. 1b, right panel).

m^6A-RIP coupled with RT-qPCR, albeit quantitative, does not offer single nucleotide resolution. A sequencing-based approach, miCLIP, provides single nucleotide m^6A mapping but lacks quantitative features [26]. To circumvent these limitations, we devised site-specific m^6A quantification by coupling m^6A antibody crosslinking with probe elongation [27]. We validated this approach by using synthetic RNAs containing A or m^6A at specific positions (Supplementary Fig. 2d). When *Hspa1a*-Fluc was examined from transfected cells, we observed an evident reduction of the "probe+1" signal at A103 in the presence of sgRNA(b) or sgRNA(c) (Fig. 1c). Since a decreased "probe+1" signal is an indication of increased methylation events, this result is in agreement with m^6A-RIP. Importantly, the same transcripts showed little difference in probe extension at A1280, a putative m^6A site in the Fluc coding region. Finally, neither the control sgRNA nor the inactive M3^{D395A}M14-dCas9 altered the level of "probe+1" signals. As an independent validation, we applied a non-antibody-based methodology to quantify the site-specific m^6A editing. The recently reported SELECT method exploits the ability of m^6A to hinder the single-base elongation activity of DNA polymerases and the nick ligation efficiency of ligases [28] (Supplementary Fig. 3a). Consistent with the antibody-based results, SELECT revealed quantitative reduction of ligated products for the targeted A103 of *Hspa1a*, but not the Fluc A1280 (Supplementary Fig. 3b). These results collectively confirmed that M3M14-dCas9 is able to achieve sgRNA-guided site-specific m^6A modification.

We noticed that, for Hsp70 5'UTR, the targeted m^6A modification efficiency is relatively low. This could be due to the high basal level of methylation at this position that limits the extent of further increase. We next chose the 5'UTR from Hsp105 that has relatively low methylation levels in MEFs as evidenced by m^6A-seq (Supplementary Fig. 4a). Further, knocking down the methyltransferase METTL3 had limited effect on the level of methylation. By contrast, silencing the demethylase FTO significantly increased the steady-state m^6A levels in the 5'UTR of Hsp105 (Supplementary Fig. 4b). Notably, the 5'UTR of

Hsp105 contains a cluster of putative m^{6}A sites, which could be targeted by the same sgRNA. We constructed a Fluc reporter bearing the mouse Hsp105 5'UTR and designed two sgRNAs targeting the m^{6}A cluster. In transfected HeLa cells, two sgRNAs each induced ~2 fold increase of 5'UTR methylation catalyzed by M3M14-dCas9 but not the inactive M3^{D395A}M14-dCas9 (Supplementary Fig. 4c). Once again, the non-targeted m^{6}A site (A1280) of the same transcript showed little difference of methylation, confirming the specificity of programmable m^{6}A modification. This encouraging result prompted us to examine whether the engineered m^{6}A "writer" is able to target the endogenous transcript in MEF cells. This was indeed the case as the same sgRNAs significantly increased the 5'UTR methylation of *Hsph1* in transfected MEFs (Fig. 1d).

Effects of targeted 5'UTR m^{6}A modification.

The 5'UTR is crucial for ribosome scanning and it is unclear whether the binding of CRISPR-Cas9 system in the 5'UTR would interfere with the normal translation process (Fig. 2a). A previous study reported that CRISPR-Cas9 targeting 5'UTR or the coding region inhibited mRNA translation by acting as a roadblock [29]. Using the Fluc reporter assay, we found that the presence of sgRNA or PAMer alone does not seem to block the ribosome scanning process despite the sequence complementarity to the 5'UTR of Hsp105 (Supplementary Fig. 5a). Additionally, co-transfection with M3M14-dCas9 had negligible effect on Fluc levels, at least under the normal growth condition (Supplementary Fig. 5b). We previously reported that 5'UTR methylation in the form of m^{6}A enables cap-independent translation under stress conditions [30,31]. We next subjected the transfected cells to heat shock stress at 42°C for 1hr, which denatured preexisting Fluc. During stress recovery, we observed an increased Fluc levels in the presence of M3M14-dCas9 when compared to the inactive mutant (Fig. 2b). Importantly, the steady-state levels of Fluc mRNA were comparable, suggesting a translational effect. The same phenomenon holds true for Hsp70 5'UTR (Fig. 2b). These results support the notion that 5'UTR m^{6}A promotes non-canonical translation when the cap-dependent mechanism is repressed.

Accumulating evidence suggests the role of m^{6}A modification in promoting mRNA degradation [32]. However, it is unclear whether the m^{6}A mark installed at different regions exhibits distinct effects. Programmable m^{6}A "writing" permits functional dissection of site-specific effects of methylation without introducing point mutations. We first assessed the effect of 5'UTR methylation on mRNA stability by taking advantage of Fluc mRNAs bearing Hsp105 5'UTR. To evaluate the turnover rate of Fluc mRNA, we treated transfected cells with the transcription inhibitor Actinomycin D for various times followed by RT-qPCR. Despite the 2 fold increase of m^{6}A in 5'UTR catalyzed by M3M14-dCas9 (Supplementary Fig. 4c), we observed little difference of mRNA turnover (Supplementary Fig. 5c). Similarly, Hsp70 5'UTR had no effects on the stability of Fluc mRNA regardless of the methylation status (Supplementary Fig. 5d). The negligible effect of 5'UTR methylation on mRNA turnover could be due to the eviction of potential m^{6}A "readers" by the scanning ribosome.

Programmable 3'UTR m^{6}A modification.

We next examined whether 3'UTR methylation induced by the engineered m^{6}A "writers" could promote mRNA degradation. The abundant β-actin mRNA contains a well-defined

m^{6}A site after the stop codon (A1216) and the moderate methylation levels (21% in HeLa cells) provide room for further m^{6}A installation (Supplementary Fig. 6a) [33]. Supporting this notion, overexpression of METT3 resulted in a 50% increase of m^{6}A at this position as measured by m^{6}A-RIP (Supplementary Fig. 6b). To examine whether a single site m^{6}A modification in the 3'UTR contributes to the degradation of *Actb*, we designed two sgRNAs and corresponding PAMers targeting A1216 (Fig. 2c). In transfected HeLa cells, only sgRNA(a) increased the methylation at A1216 (~3 fold) as quantified by m^{6}A-RIP (Fig. 2c). As an independent validation, we conducted site-specific m^{6}A quantification. Indeed, only sgRNA(a) reduced the "probe+1" signal at A1216 of β-actin mRNA, corresponding to the increased methylation (Fig. 2d). Notably, the same sample showed little difference of methylation at A2577 of *Malat1*, a non-coding RNA as a non-targeting internal control (Fig. 2d). To substantiate the targeting specificity of m^{6}A modification by the engineered m^{6}A writer, we applied SELECT to the same samples and observed significant reduction of ligated products by sgRNA(a), an indication of increased m^{6}A levels (Supplementary Fig. 6c).

Although ectopic expression of M3M14-dCas9 does not seem to alter global RNA methylation (Supplementary Fig. 2c), it is unclear whether the presence of particular sgRNAs leads to off-targeting of m^{6}A methylation. To assess the off-targeting possibility of *Actb*-specific sgRNA(a) across the transcriptome, we conducted optimized m^{6}A-seq. With improved resolution (Supplementary Fig. 7a and 7b), we compared the entire m^{6}A methylome in cells expressing active or inactive m^{6}A writer, in the presence of targeted sgRNA or λ2 sgRNA control. The overall m^{6}A landscapes across the transcriptome are comparable in these cells (Supplementary Fig. 7c). Pair-wise comparison of individual m^{6}A sites showed limited variation (Supplementary Fig. 7d). Importantly, the targeted site of *Actb* showed an evident increase of m^{6}A density in cells expressing M3M14-dCas9 when compared to the inactive mutant (Supplementary Fig. 7e). Although different sgRNAs could have different outcomes, the possible off-target of sgRNA-guided m^{6}A writers is either negligible or beyond the detection threshold.

Having achieved site-specific 3'UTR m^{6}A modification of β-actin mRNA by sgRNA(a), we next examined the stability of endogenous *Actb* in these cells. Remarkably, the half-life of *Actb* was significantly reduced in the presence of MTase-dCas9, but not MTase^{D395A}-dCas9 (Fig. 2d). Notably, the non-targeted transcript *Gapdh* maintained its stability in the same samples (Supplementary Fig. 7f). The correlation between sgRNA(a)-guided m^{6}A installation and increased mRNA turnover suggests that a single m^{6}A modification at 3'UTR influences the mRNA stability.

Designing programmable m^{6}A erasers.

To fully interrogate the regional effect of m^{6}A modification, it is highly desirable to achieve targeted erasure of m^{6}A from mRNA using engineered demethylases. Two members of the α-ketoglutarate-dependent dioxygenases protein family, FTO and ALKBH5, have been shown to act as m^{6}A demethylases [6,7]. Unlike m^{6}A "writers" that require consensus motif for targeting, the substrate specificity of ALKBH5 and FTO seems to rely on conformational markers signified by m^{6}A [34]. In addition to internal m^{6}A, FTO can also demethylase m^{6}Am

adjacent to the 5'end cap [35,36]. Since the non-AlkB domains are crucial in the functionality of both demethylases, we fused the full length ALKBH5 or FTO to the amino terminus of dCas9 (Fig. 3a). To generate inactive controls, we introduced H204A mutation to ALKBH5 and (H231A, D233A) double mutations to FTO (Supplementary Fig. 8a and 8d). These fusion proteins primarily localized in the nucleus of transfected cells as expected (Supplementary Fig. 8b and 8e). Notably, overexpression of these engineered "erasers" alone did not alter global m^6A levels in transfected cells (Supplementary Fig. 8c and 8f). To assess the off-targeting effect, we conducted optimized m^6A-seq and compared the entire m^6A methylome in cells expressing active or inactive FTO-dCas9, in the presence of targeted sgRNA or $\lambda 2$ sgRNA control. The overall m^6A landscapes across the transcriptome are comparable in these cells (Supplementary Fig. 9a). Pair-wise comparison of individual m^6A sites showed that the global variation in the presence of targeted sgRNA is no greater than the control (Supplementary Fig. 9b).

To evaluate the sgRNA-guided demethylation activity of ALKBH5-dCas9 and FTO-dCas9, we chose to target *Malat1* because this abundant long non-coding RNA exhibits a high degree of methylation at A2577 (80% in HeLa cells) (Supplementary Fig. 10a) [33]. We designed two sgRNAs and corresponding PAMers targeting A2577 of *Malat1*. Interestingly, only sgRNA(a) was able to reduce its methylation when co-expressed with either ALKBH5-dCas9 or FTO-dCas9 (Fig. 3b). This was due to the demethylase activity of engineered m^6A erasers because inactive mutants of ALKBH5 (Fig. 3c) and FTO (Fig. 3e) did not alter the m^6A signal at A2577 of *Malat1*. Importantly, the m^6A levels at A1216 of *Actb* were comparable in the presence of sgRNA(a) targeting *Malat1*. The high specificity of ALKBH5-dCas9 and FTO-dCas9 was further confirmed using site-specific m^6A quantification (Fig. 3d and 3f), including SELECT (Fig. 4a and 4b).

m^6A editing of *Malat1* acts as a structural switch

It is intriguing to find that only sgRNA(a) enables site-specific *Malat1* demethylation. m^6A at A2577 has been reported to act as a structural switch for *Malat1* by destabilizing the stem structure [37]. As a result, the exposed U-tract allows subsequent binding of HNRNPC (Fig. 4c and Supplementary Fig. 10b). Since sgRNA(b) is located upstream of the U-tract, it is possible that the presence of HNRNPC prevents the access of engineered m^6A "erasers" to the target site. As an independent means to evaluate the methylation status of *Malat1*, we conducted HNRNPC immunoprecipitation coupled with RT-qPCR of *Malat1*. Once again, only sgRNA(a) significantly reduced the *Malat1*-associated HNRPNC (Fig. 4c), confirming the functional consequence of m^6A erasure from A2577 of *Malat1*. This result implies that m^6A editing has the potential to control interactions of RNA-binding proteins by remodeling RNA structures. The comparable catalytic activities between ALKBH5-dCas9 and FTO-dCas9 also indicate that FTO is capable of targeting internal m^6A.

Discussion

A grand challenge in the post-genomic era is to elucidate the complex layers of epigenetic control of gene expression. Over the past thirty years, much research has been conducted on how DNA methylation and histones modifications (the 'epigenome') regulate gene

expression [16,17]. More recently, RNA modifications have been discovered that decorate all RNA species across many living organisms. Dynamic and reversible RNA modifications constitute the "epitranscriptome", a tunable layer influencing nearly all aspects of RNA metabolism and functionality [1,2]. Much of our current knowledge about RNA post-transcriptional modifications is limited to studies that rely on genetic perturbations that affect global RNA methylation as a whole. Although these results are informative for implicating the significance of RNA markers in cellular regulation, they are too limited for detailed mechanistic dissection. Additionally, the asymmetric m⁶A deposition suggests that regional methylation may have distinct functional consequences. To interrogate the site-specific effect of m⁶A, point mutation is a common methodology to permanently remove the modification site. However, we lack an approach to m⁶A installation in a site-specific manner.

By coupling CRISPR-Cas9 technology, the m⁶A editors described here offer researchers a versatile toolbox to unlock the secrets of epitranscriptome. For the first time, it is now possible to achieve site-specific m⁶A installation or erasure, which is key to understanding the regional effects of mRNA methylation. We confirmed that a single site 5'UTR methylation enables non-canonical mRNA translation. By contrast, manipulating 3'UTR methylation influences mRNA turnover but not in an exclusive manner. One important application of m⁶A editing is to alter RNA secondary structures without changing the primary sequence. By site-specific m⁶A editing, certain m⁶A-dependent RNA structural switches can now be remodeled, offering a powerful approach to fine-tuning specific RNA-protein interactions. With the versatility of CRISPR-Cas enzymes on the rise [15], it is conceivable to construct m⁶A editors with smaller size, higher specificity, and more adjustable features like the one inducible by small molecules. Given the broad range of chemical modifications in cellular RNAs, our approach also serves as a prototype for developing toolkits capable of editing diverse base or sugar modifications of RNA molecules.

Methods

Cell lines and reagents

MEF, HeLa and HEK293 cells were maintained in Dulbecco's Modification of Eagle's Medium (Corning 10–013-CV) with 10% Fetal Bovine Serum (FBS, Sigma 12306C). Antibodies used in the western blot are listed below: anti-ALKBH5 (Millipore ABE1013), anti-FTO (Phosphosolutions 597-Fto), anti-METTL3 (Proteintech 15073–1-AP), anti-Cas9 (Millipore MAC133), anti-HNRNPC (Santa cruz sc-32308) and anti-β-Actin (Sigma A5441).

Plasmid constructions and PAMmer synthesis

Full-length CDS of human *METTL3* and *METL14* were cloned into pcDNA3.1 (Invitrogen) to generate pcDNA-Mettl3 and pcDNA-Mettl14 plasmids. DNA sequences encoding methytransferase domain of METTL3 (residue 369–580) and METTL14 (residue 116–402) were amplified from pcDNA-Mettl3 and pcDNA-Mettl14, respectively, and subcloned into pCMV-BE2 vector backbone (Addgene #73020) using Gibson assembly (NEB E2611S).

The resulting plasmid was used as a template to produce the methytransferase inactive mutant plasmid (M3^{D395A}M14-dCas9) using Q5® Site-Directed Mutagenesis Kit (NEB E0554S). Full-length coding sequences of human ALKBH5 and FTO were directly cloned into BE2 vector using *Not* I and *Sma* I to generate ALKBH5-dCas9 and FTO-dCas9. The UGI sequences were removed from both vectors. The resulting plasmids were used as templates to generate the demethylase inactive mutant plasmids (ALKBH5H204A-dCas9 and FTOH231A/D233A-dCas9) using Q5® Site-Directed Mutagenesis Kit (NEB E0554S). To purify M3M14 fusion protein from bacteria, M3M14 DNA sequence was amplified from M3M14-dCas9 and subcloned into pGEX-6P-1 vector using *Xho* I and *Not* I. sgRNAs were designed based on the target m^{6}A site for individual RNA and cloned into Cas9 sgRNA vector (Addgene #68463). PAMmers were designed based on the principles as previously described (Connell et al 2014 and Nelles et al 2016). The HPLC-purified PAMer sequences consisting of mixed DNA and 2'OMe RNA bases were commercially synthesized by Integrated DNA Technologies. DNA sequences of all primers, sgRNAs and PAMers used in this study are listed in the Supplementary Dataset 1.

In vitro methylation assay

The RNA probe (5'-CGAUCCUCGGCCA<u>GGAC</u>CAGCCUUCCCCAG-3') derived from *Hsp70* 5'UTR was commercially synthesized *in vitro* (Thermo Fisher Scientific). Fusion proteins of M3M14, M14M3 and their catalytically inactive forms were purified from bacteria. The *in vitro* methylation assay was performed in a 50 μl reaction mixture containing 400 nM RNA probe, 20 mM Tris (pH 7.5), 50 μM ZnCl$_2$, 1 mM DTT, 0.01% Triton-X, 0.2 U/μL RNaseOUT, 1% glycerol, 0.5 μCi [methyl-^{3}H]AdoMet (PerkinElmer) and 100 nM purified protein. The reaction was incubated at 30°C for 1 h and then stopped by adding Trizol reagent (Invitrogen). RNA after reaction was precipitated and purified using sodium acetate at −20°C for at least 2 h. The precipitated RNA was subjected to radioactivity measurement using scintillation counting (Beckman). Levels of ^{3}H-methyl-incorporated RNA are shown as disintegrations per minute (DPM). The methylation assay data are shown as mean ± s.e.m. from three independent replicates.

Cell transfection for RNA m^{6}A editing

MEF or HeLa cells were grown and passaged in 10-cm culture plate at approximately 80% confluency. For targeted methylation of the m^{6}A sites in exogenously expressed *Hsp70* 5'UTR-Luc and *Hsp105* 5'UTR-Luc mRNA, cells were co-transfected with either M3M14-dCas9 or M3^{D395A}M14-dCas9, sgRNA and Fluc reporter plasmids at a mass ratio of 5:3:1 using Lipofectamine 2000 (Life Technologies) according to the manufacturer's instructions. For targeted methylation of the endogenous m^{6}A sites of *Hsp105* 5'UTR and *β-Actin* 3'UTR cells were co-transfected with M3M14-dCas9 or M3^{D395A}M14-dCas9 and sgRNA at a mass ratio of 5:3 using Lipofectamine 2000. For targeted demethylation of the m^{6}A sites in *Malat1*, cells were co-transfected with ALKBH5-dCas9, or FTO-dCas9, or their mutants, and sgRNA plasmids at a mass ratio of 3:1 using Lipofectamine 2000. PAMmers were transfected using Lipofectamine RNAiMax (Life Technologies) according to manufacturer's instructions. 36–48 h after transfection, cells were washed with PBS followed by RNA isolation for m^{6}A immunoprecipitation.

m^{6}A immunoprecipitation

Total RNA was isolated using Trizol reagent followed by fragmentation using freshly prepared RNA fragmentation buffer (10 mM Tris-HCl pH 7.0, 10 mM ZnCl$_2$). 180 µg fragmented RNA was incubated with 6 µg anti-m^{6}A antibody in 1× m^{6}A IP buffer (10 mM Tris-HCl pH 7.4, 150 mM NaCl, and 0.1% Igepal CA-630) supplemented with 6 µL RNase OUT (40 U/µL) and 2 mM RVC for 2 h at 4°C. The m^{6}A-IP mixture was then incubated with Protein A/G beads and rotated for additional 3 h at 4°C. Following four washes in 1× IP buffer, m^{6}A-containing RNA fragments were eluted by incubation with 200 µl elution buffer (6.7 mM N^6-methyladenosine 5'-monophosphate sodium salt in 1× IP buffer) for 1 h at 4°C. Eluted RNA was used for further RT-qPCR.

Immunofluorescence staining

Cells grown on glass coverslips were fixed in 4% paraformaldehyde for 10 min at 4°C. After permeabilization in 0.2% Triton X-100 for 5 min at room temperature, the cover slips were blocked with 1% BSA for 1 h. Cells were stained with anti-Cas9 antibody (Millipore MAC133) overnight at 4°C, followed by incubation with Alexa Fluor 546 donkey anti-mouse secondary antibody for 1 h at room temperature. The nuclei were counter-stained with DAPI (1:1,000 dilution) for 10 min. Cover slips were mounted onto slides and visualized using a Zeiss LSM710 confocal microscope.

Western blot

Cells were harvested by adding SDS sample buffer (50mM Tris pH 6.8, 100mM dithiothreitol, 2% SDS, 0.1% bromophenol blue, 10% glycerol) and heated for 10 min at 95°C. Proteins were separated on SDS-PAGE and transferred to Immobilon-P membranes (Millipore). Membranes were blocked for 1 h in TBS containing 5% non-fat milk and 0.1% Tween-20, followed by incubation with primary antibodies overnight at 4°C. After incubation with horseradish-peroxidase-coupled secondary antibodies at room temperature for 1 h, immunoblots were visualized using enhanced chemiluminescence (ECL Plus, GE Healthcare).

RT-qPCR

Total RNA was isolated by Trizol reagent and used for reverse transcription assay via High Capacity cDNA Reverse Transcription Kit (Invitrogen). Real-time PCR analysis was conducted using Power SYBR Green PCR Master Mix (Applied Biosystems) and carried on a LightCycler 480 Real-Time PCR System (Roche Applied Science). Primers used in qPCR assay are listed in the Supplementary Dataset 1.

m^{6}A site-specific detection

Total RNA was isolated from cells 36–48 h after transfection with components for targeted methylation of *Hsp70 5'UTR* and *β-actin* or demethylation of *Malat1*. In detail, 20 µg total RNA was diluted in 450 µl immunoprecipitation buffer (50 mM Tris, pH 7.4, 100 mM NaCl, 0.05% NP-40) and incubated with 1 µg m^{6}A antibody at 4°C for 2 h, rotating head over tail. The antibody-RNA mixture was then crosslinked twice under the conditions of UV 254 nm 0.15 J/cm2 in a Stratalinker (Agilent), followed by precipitation of RNA in 1 ml ethanol and

45 μl sodium acetate. Reverse transcription was performed in a total volume of 7 μl reaction containing m^6A-crosslinked RNA, Tth buffer (Promega) and 50 pmole primer. The sequences of the primers targeting m^6A sites were listed as follows: Primer targeting *Hspa1a* 5'UTR, 5'- AGGGATGCTCTGGGGAAGGCTGG-3'; Primer targeting Fluc coding region: 5'-GCGGTCAACGATGAAGAAGTGTTCGTCTTCG-3. Primer targeting *Actb*, 5'-CAAGAAAGGGTGTAACGCAACTAAGTCATAG-3'; Primer targeting *Malat1*, 5'-CAATTAATGCTAGTCCTCAGGATTTAAAAAATAATCTTAACTCAAAG-3'. Subsequently the reaction mixture was heated at 95°C for 10 min and gradually cooled to room temperature. Following annealing, 5 U of Tth enzyme and 1 mM $MnCl_2$ were added into the mixture and heated at 70°C for 3 min. Primer extension was initiated by addition of 1 μM Fluorescein-12-dUTP and reacted for 15 min at 70°C. The RT products were resolved on a 15% Novex TBE-Urea gels (Thermo Fisher Scientific) and FAM signal was detected by Typhoon 9400 variable mode imager.

SELECT for detection of m^6A

5 ug total RNA was incubated with 40 nM Up Primer, 40 nM Down Primer and 5 μM dNTP in 17 μl 1×CutSmart buffer (50 mM KAc, 20 mM Tris-HAc, 10 mM MgAc2, 100 μg/ml BSA) and annealed at a temperature gradient: 90°C for 1min, 80°C for 1min, 70°C for 1min, 60°C for 1min, 50°C for 1min, and then 40°C for 6min. Subsequently, the 17 μl annealing products were incubated with a 3 μl of enzyme mixture containing 0.01 U Bst 2.0 DNA polymerase, 0.5 U SplintR ligase and 10 nmol ATP. The final 20 μl reaction mixture was incubated at 40°C for 20 min, denatured at 80°C for 20 min and kept at 4°C. Real-time PCR analysis was conducted using Power SYBR Green PCR Master Mix (Applied Biosystems) and carried on a LightCycler 480 Real-Time PCR System (Roche Applied Science) as described. qPCR was run at the following condition: 95°C, 5min; (95°C, 10s; 60°C, 45s)×40 cycles. The SELECT products of indicated site were normalized to the RNA abundance of indicated transcript bearing this site. Primers used in SELECT assay are listed in the Supplementary Dataset 1.

m^6A dot blot

RNA was isolated from transfected cells. Equal amount of RNA were dropped on a nylon membrane (Thermo Fisher Scientific) followed by crosslinking under the conditions of UV254 nm, 0.12 J/cm^2. The membrane was blocked in PBST (5% non-fat milk and 0.1 % Tween-20) for 1 hr and subsequently incubated with anti-m^6A antibody (1:1000 dilution) overnight at 4°C. After washing 3 times in PBST buffer, the membrane was incubated with HRP-conjugated anti-rabbit IgG (1:5000 dilution) for 1 hr and visualized by using enhanced chemiluminescence (ECL Plus, GE Healthcare).

RNA immunoprecipitation

For detection of M3M14-dCas9-sgRNA complex binding to target RNA sequence, HeLa cells were co-transfected with *Hsph1*-Fluc, M3M14-dCas9, control or target sgRNA, and increasing dose of PAMer. For detection of hnRNP-C binding to *MALAT1*, cells were transfected with target sgRNA, PAMer, either control dCas9 or ALKBH5-dCas9 or FTO-dCas9. 36 h after transfection, cells were incubated with the growth media containing 1% formaldehyde for 10 min at room temperature, followed by termination of cross-link

reaction by adding 0.25 M glycine (pH 7.5). Then the cells were washed twice with cold PBS and scraped from the plates in cold PBS. The cell suspension was centrifuged at 5000 rpm for 4 min to pellet the cells. The cell pellets were washed once more and resuspended in 200 μl lysis buffer B (50 mM Tris-HCl pH 7.5, 150 mM KCl, 5mM EDTA, 1% NP40, 0.1% SDS, 0.5% sodium deoxycholate, 50 mM NaF, protease inhibitor and RNase OUT) by pipetting up and down. The cell lysate was sonicated for 7 min a Bioruptor sonicator (15 sec ON, 30 sec OFF), followed by addition of 300 μl RIPA buffer (50 mM Tris-HCl pH7.5, 150 mM KCl, 1% NP40, 50 mM NaF and protease inhibitor). Insoluble cell debris was pelleted after centrifugation for 10 min at full speed. Normal IgG and Protein A/G bead slurry were added to each 500 μl supernatant to remove nonspecific binding. The pre-cleared lysates were incubated with additional 2.5 μl RNaseOUT and Protein A/G bead slurry pre-coated with anti-Cas9 or anti-hnRNP-C antibody at 4°C for overnight. The beads were washed in RIPA wash buffer (50 mM Tris-HCl pH7.5, 150 mM KCl, 1% NP40, 0.25% sodium deoxycholate) for 5 times and TE buffer (10 mM Tris-HCl pH7.5, 1 mM EDTA) for additional 2 times. The rinsed beads were then treated with TURBO DNase (Life Technologies) and eluted in RIPA elution buffer (50 mM Tris-HCl pH7.5, 1 mM EDTA, 10 mM DTT, 1% SDS and RNaseOUT), followed by reverse crosslinking at 70°C for 5 h and proteinase K digestion. Trizol reagent was added to the bead supernatant to isolate RNA. The RNA was precipitated using isopropanol and reverse transcribed using High Capacity cDNA Reverse Transcription Kit (Invitrogen) using random hexamer primers. RT products were used for PCR or qPCR.

Real-time luciferase assay

Cells were grown in 35-mm dishes and transfected with indicated plasmids. 10 min after transfection, luciferase substrate D-luciferin (1 mM, Regis Tech) was added into the culture medium. Luciferase activity was monitored and recorded in a real-time manner using Kronos Dio Luminometer (Atto).

mRNA stability assay

Cells were treated with transcription inhibitor actinomycin D and collected at different times (0 h, 1 h, 3 h and 6 h). RNA spike-in control (*in vitro*-synthesized mRNA) was added proportional to the total cell numbers and total RNA was isolated by Trizol reagent. After reverse transcription, the mRNA levels of transcripts of interest were detected by real-time quantitative PCR.

m6A-seq

Total RNA was isolated using Trizol reagent followed by fragmentation in RNA fragmentation buffer (10 mM Tris-HCl, pH 7.0, 10 mM $ZnCl_2$). Approximately 400 μg fragmented RNA was incubated with 6 μg anti- m6A antibody (Synaptic Systems 200 203) and 8 μg anti-m6A antibody Abcam ab151230) in IP buffer (10 mM Tris-HCl, pH 7.4, 150 mM NaCl, and 0.1% Igepal CA-630) for 2 h at 4°C. The antibody-RNA mixture was then incubated with Protein A/G beads for additional 2 h at 4°C with rotation. After washing 3 times with IP buffer, bound RNA was eluted using 100 μL elution buffer (6.7 mM N^6-Methyladenosine 5'-monophosphate sodium salt in IP buffer), followed by ethanol

precipitation. Precipitated RNA was used for cDNA library construction and high-throughput sequencing described below.

cDNA library construction

m[6]A-containing RNAs (m[6]A-seq) or fragmented total RNAs (RNA-seq) were dephosphorylated for 1 hr at 37°C in 15 μl reaction (1× T4 polynucleotide kinase buffer, 10 U SUPERase_In and 20 U T4 polynucleotide kinase). The products were separated on a 15 % polyacrylamide TBE-urea gel (Invitrogen) and visualized using SYBR Gold (Invitrogen). The gel with selected regions 40–60 nt was excised and disrupted by using centrifugation through the holes at the bottom of the tube. RNA fragments were dissolved by soaking overnight in 400 μl gel elution buffer (300 mM NaOAc, pH 5.5, 1 mM EDTA, 0.1 U/ml SUPERase_In). The gel debris was removed using a Spin-X column (Corning), followed by ethanol precipitation. Purified RNA fragments were re-suspended in nuclease-free water. Poly-(A) tailing reaction was carried out for 45 min at 37°C (1 × poly-(A) polymerase buffer, 1 mM ATP, 0.75 U/μl SUPERase_ In and 3 U *E. coli* poly-(A) polymerase).

For reverse transcription, the following oligos containing barcodes were used:

MCA02: 5'-pCAGATCGTCGGACTGTAGAACTCTCAAGCAGAAGACGGCATACGATTT TTTTTTTTTTTTTTTTTTVN-3';

LGT03: 5'-pGTGATCGTCGGACTGTAGAACTCTCAAGCAGAAGACGGCATACGATT TTTTTTTTTTTTTTTTTTTVN-3';

YAG04: 5'-pAGGATCGTCGGACTGTAGAACTCTCAAGCAGAAGACGGCATACGATT TTTTTTTTTTTTTTTTTTTVN-3';

HTC05: 5'-pTCGATCGTCGGACTGTAGAACTCTCAAGCAGAAGACGGCATACGATT TTTTTTTTTTTTTTTTTTTVN-3'.

In brief, the tailed-RNA sample was mixed with 0.5 mM dNTP and 2.5 mM synthesized primer and incubated at 65°C for 5 min, followed by incubation on ice for 5 min. The reaction mix was then added with 20 mM Tris (pH 8.4), 50 mM KCl, 5 mM MgCl$_2$, 10 mM DTT, 40 U RNaseOUT and 200 U SuperScript III. Reverse transcription reaction was performed according to the manufacturer's instruction. Reverse transcription products were separated on a 10% polyacrylamide TBE-urea gel as described earlier. The extended first-strand product band was expected to be approximately 100–150 nt, and the corresponding region was excised. The cDNA was recovered by using DNA gel elution buffer (300 mM NaCl, 1 mM EDTA). First-strand cDNA was circularized in 20 μl of reaction containing 1× CircLigase buffer, 2.5 mM MnCl$_2$, 1M Betaine, and 100 U CircLigase II (Epicentre). Circularization was performed at 60°C for 1 h followed by inactivation at 80°C for 10 min. The circularized cDNA was recovered after precipitation in ethanol and used as template for PCR.

Deep sequencing

Single-stranded template was amplified by PCR by using the Phusion High-Fidelity enzyme (NEB) according to the manufacturer's instructions. The oligonucleotide primers qNTI200 (5'-CAAGCAGAAGACGGCATA- 3') and qNTI201 (5'-AATGATACGGCGACCACCG ACAGGTTCAGAGTTCTACAGTCCGACG- 3') were used to create DNA suitable for sequencing, i.e., DNA with Illumina cluster generation sequences on each end and a sequencing primer binding site. The PCR contains $1\times$ HF buffer, 0.2 mM dNTP, 0.5 μM oligonucleotide primers, and 0.5 U Phusion polymerase. PCR was carried out with an initial 30 s denaturation at 98°C, followed by 12 cycles of 10 s denaturation at 98°C, 20 s annealing at 60°C, and 10 s extension at 72°C. PCR products were separated on a nondenaturing 8% polyacrylamide TBE gel as described earlier. Expected DNA at 140 bp was excised and recovered as described. After quantification by Agilent BioAnalyzer DNA 1000 assay, equal amount of barcoded samples were pooled into one sample. Approximately 3–5 pM mixed DNA samples were used for cluster generation followed by deep sequencing by using sequencing primer 5'-CGACAGGTTCAGAGTTCTACAGTCCGACGATC-3' (Illumina HiSeq).

m⁶A peak calling

The sequencing reads, after trimmed 3' adaptor and low quality bases, were aligned to human transcriptome, using Bowtie with parameters: -a --best -m1 --strata. The annotation file downloaded from ENSEMBL database (GRCh38) was used to construct the transcriptome index file. For each gene, the transcript with the longest CDS was selected. In the case of equal CDS length, the longest transcript was used. For read alignment, a maximum of two mismatches were permitted. To avoid ambiguous, the reads mapped to multiple positions were disregarded for further analyses.

We used a non-parameter method to predict m⁶A sites on transcripts. In brief, a sliding window of 50 nucleotides with a step of 25 nucleotides was employed to scan each transcript. For each window with maximum read coverage higher than 10, a peak-over-median score (POM) was derived by calculating the ratio of the mean read coverage in the window to the median read coverage of corresponding transcript. The windows with POM higher than 3 in IP sample were obtained. The same processes were performed in input sample. The windows found in input sample were eliminated from following analyses. The windows that overlapped at least single nucleotide were merged into one cluster. Finally, a peak over input (POI) score was assigned to each cluster by calculating the ratio of POM in the IP sample to that in the input sample. The cluster with POI score higher than 3 were retrieved, and defined as m⁶A-enriched cluster. The peak position with maximum coverage in each m⁶A-enriched cluster was defined as the position of m⁶A peak. The adenosine site of the nearest RRAC motif was defined as m⁶A residue. To reduce noises for background reads and bias from peak calling method, only the m⁶A sites that were found in all biological replicates were used. The coverage of m⁶A site was defined as Reads Per Kilobase Million (RPKM) value surrounding m⁶A sites from −50 nt to +50 nt.

Author Manuscript

Supplementary Material

Refer to Web version on PubMed Central for supplementary material.

Acknowledgements

References

1. Roundtree IA, Evans ME, Pan T & He C Dynamic RNA Modifications in Gene Expression Regulation. Cell 169, 1187–1200 (2017). [PubMed: 28622506]

2. Lewis CJ, Pan T & Kalsotra A RNA modifications and structures cooperate to guide RNA-protein interactions. Nat Rev Mol Cell Biol 18, 202–210 (2017). [PubMed: 28144031]

3. Bokar JA, Shambaugh ME, Polayes D, Matera AG & Rottman FM Purification and cDNA cloning of the AdoMet-binding subunit of the human mRNA (N6-adenosine)-methyltransferase. RNA 3, 1233–1247 (1997). [PubMed: 9409616]

4. Liu J, et al. A METTL3-METTL14 complex mediates mammalian nuclear RNA N6-adenosine methylation. Nat Chem Biol 10, 93–95 (2014). [PubMed: 24316715]

5. Ping XL, et al. Mammalian WTAP is a regulatory subunit of the RNA N6-methyladenosine methyltransferase. Cell Res 24, 177–189 (2014). [PubMed: 24407421]

6. Jia G, et al. N6-methyladenosine in nuclear RNA is a major substrate of the obesity-associated FTO. Nat Chem Biol 7, 885–887 (2011). [PubMed: 22002720]

7. Zheng G, et al. ALKBH5 is a mammalian RNA demethylase that impacts RNA metabolism and mouse fertility. Mol Cell 49, 18–29 (2013). [PubMed: 23177736]

8. Fu Y, Dominissini D, Rechavi G & He C Gene expression regulation mediated through reversible m(6)A RNA methylation. Nat Rev Genet 15, 293–306 (2014). [PubMed: 24662220]

9. Meyer KD & Jaffrey SR The dynamic epitranscriptome: N6-methyladenosine and gene expression control. Nat Rev Mol Cell Biol 15, 313–326 (2014). [PubMed: 24713629]

10. Edupuganti RR, et al. N(6)-methyladenosine (m(6)A) recruits and repels proteins to regulate mRNA homeostasis. Nat Struct Mol Biol 24, 870–878 (2017). [PubMed: 28869609]

11. Meyer KD, et al. Comprehensive analysis of mRNA methylation reveals enrichment in 3' UTRs and near stop codons. Cell 149, 1635–1646 (2012). [PubMed: 22608085]

12. Dominissini D, et al. Topology of the human and mouse m6A RNA methylomes revealed by m6A-seq. Nature 485, 201–206 (2012). [PubMed: 22575960]

13. Hsu PD, Lander ES & Zhang F Development and applications of CRISPR-Cas9 for genome engineering. Cell 157, 1262–1278 (2014). [PubMed: 24906146]

14. Doudna JA & Charpentier E Genome editing. The new frontier of genome engineering with CRISPR-Cas9. Science 346, 1258096 (2014). [PubMed: 25430774]

15. Komor AC, Badran AH & Liu DR CRISPR-Based Technologies for the Manipulation of Eukaryotic Genomes. Cell 169, 559 (2017).

16. Stricker SH, Koferle A & Beck S From profiles to function in epigenomics. Nat Rev Genet 18, 51–66 (2017). [PubMed: 27867193]

17. Allis CD & Jenuwein T The molecular hallmarks of epigenetic control. Nat Rev Genet 17, 487–500 (2016). [PubMed: 27346641]

18. Liu XS, et al. Editing DNA Methylation in the Mammalian Genome. Cell 167, 233–247 e217 (2016). [PubMed: 27662091]

19. Morita S, et al. Targeted DNA demethylation in vivo using dCas9-peptide repeat and scFv-TET1 catalytic domain fusions. Nat Biotechnol 34, 1060–1065 (2016). [PubMed: 27571369]

20. Nelles DA, et al. Programmable RNA Tracking in Live Cells with CRISPR/Cas9. Cell 165, 488–496 (2016). [PubMed: 26997482]

21. O'Connell MR, et al. Programmable RNA recognition and cleavage by CRISPR/Cas9. Nature 516, 263–266 (2014). [PubMed: 25274302]

22. Wang X, et al. Structural basis of N(6)-adenosine methylation by the METTL3-METTL14 complex. Nature 534, 575–578 (2016). [PubMed: 27281194]

23. Wang P, Doxtader KA & Nam Y Structural Basis for Cooperative Function of Mettl3 and Mettl14 Methyltransferases. Mol Cell 63, 306–317 (2016). [PubMed: 27373337]

24. Komor AC, Kim YB, Packer MS, Zuris JA & Liu DR Programmable editing of a target base in genomic DNA without double-stranded DNA cleavage. Nature 533, 420–424 (2016). [PubMed: 27096365]

25. Ke S, et al. m6A mRNA modifications are deposited in nascent pre-mRNA and are not required for splicing but do specify cytoplasmic turnover. Genes Dev 31, 990–1006 (2017). [PubMed: 28637692]

26. Linder B, et al. Single-nucleotide-resolution mapping of m6A and m6Am throughout the transcriptome. Nat Methods 12, 767–772 (2015). [PubMed: 26121403]

27. Zhou J, et al. N(6)-Methyladenosine Guides mRNA Alternative Translation during Integrated Stress Response. Mol Cell 69, 636–647 e637 (2018). [PubMed: 29429926]

28. Xiao Y, et al. An Elongation- and Ligation-Based qPCR Amplification Method for the Radiolabeling-Free Detection of Locus-Specific N(6)-Methyladenosine Modification. Angew Chem Int Ed Engl 57, 15995–16000 (2018). [PubMed: 30345651]

29. Liu Y, et al. Targeting cellular mRNAs translation by CRISPR-Cas9. Sci Rep 6, 29652 (2016). [PubMed: 27405721]

30. Meyer KD, et al. 5' UTR m(6)A Promotes Cap-Independent Translation. Cell 163, 999–1010 (2015). [PubMed: 26593424]

31. Zhou J, et al. Dynamic m(6)A mRNA methylation directs translational control of heat shock response. Nature 526, 591–594 (2015). [PubMed: 26458103]

32. Wang X, et al. N6-methyladenosine-dependent regulation of messenger RNA stability. Nature 505, 117–120 (2014). [PubMed: 24284625]

33. Liu N, et al. Probing N6-methyladenosine RNA modification status at single nucleotide resolution in mRNA and long noncoding RNA. RNA 19, 1848–1856 (2013). [PubMed: 24141618]

34. Zou S, et al. N(6)-Methyladenosine: a conformational marker that regulates the substrate specificity of human demethylases FTO and ALKBH5. Sci Rep 6, 25677 (2016). [PubMed: 27156733]

35. Mauer J, et al. Reversible methylation of m6Am in the 5' cap controls mRNA stability. Nature 541, 371–375 (2017). [PubMed: 28002401]

36. Wei J, et al. Differential m(6)A, m(6)Am, and m(1)A Demethylation Mediated by FTO in the Cell Nucleus and Cytoplasm. Mol Cell 71, 973–985 e975 (2018). [PubMed: 30197295]

37. Liu N, et al. N(6)-methyladenosine-dependent RNA structural switches regulate RNA-protein interactions. Nature 518, 560–564 (2015). [PubMed: 25719671]
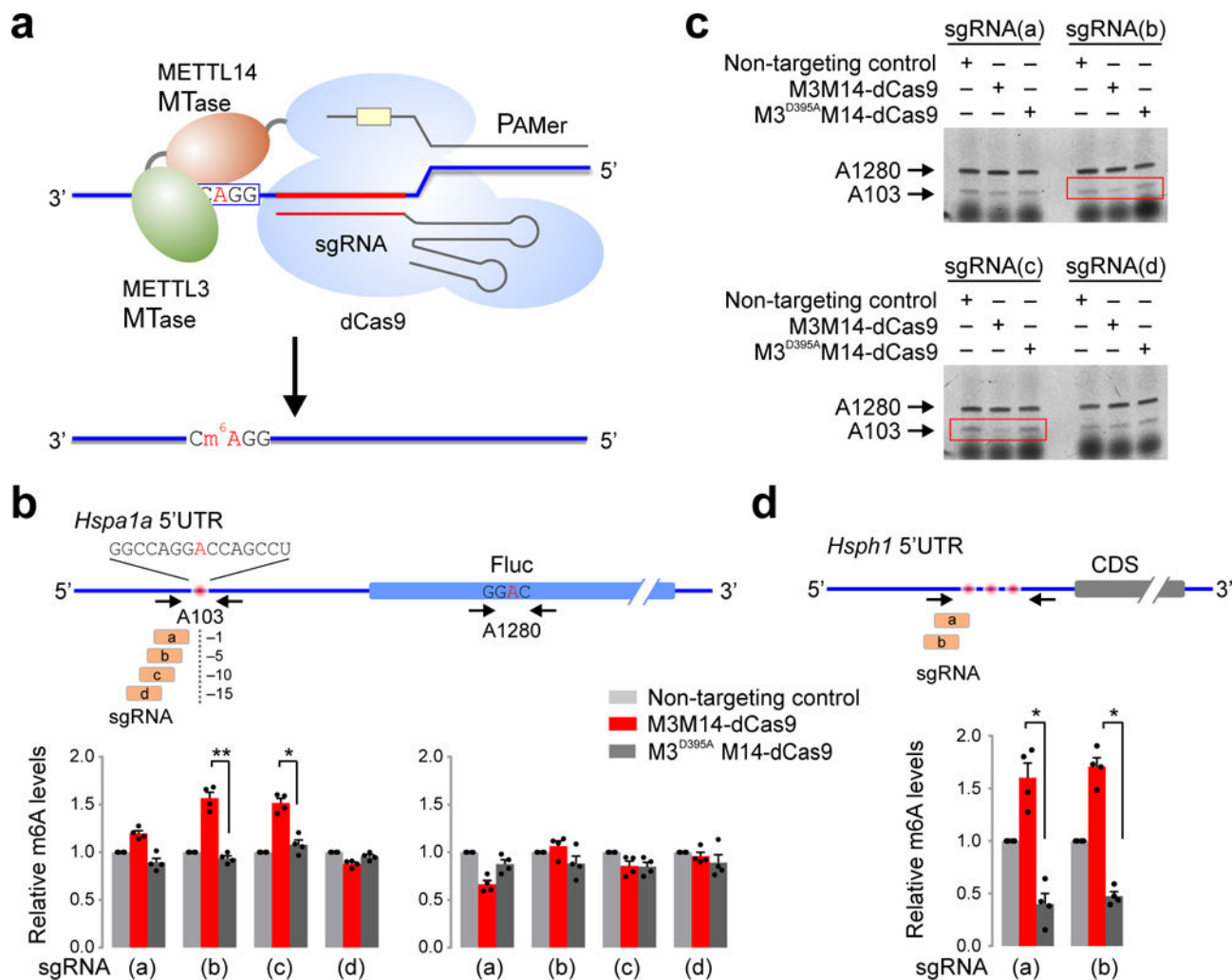
Figure 1 |. Targeted 5'UTR methylation by engineered m⁶A "writers".

a. Schematic of engineered m^{6}A "writers" by coupling CRISPR-dCas9 with single chain methyltransferase domains derived from METTL3 (green) and METTL14 (brown). The sgRNA and PAMmer are base-paired to nearby regions of the m^{6}A consensus motif on target RNA. PAMer supplies the PAM sequence NGG that does not need to be present on target RNA. **b.** Measurement of m^{6}A levels on *Hspa1a* 5'UTR-Luc in transfected HeLa cells. λ2 sgRNA was used as the non-targeting control. Primers were designed to span the targeting m^{6}A site A103 in *Hspa1a* 5'UTR or A1280 of Fluc mRNA as control for off-targeting. Error bars, mean ± s.e.m.; unpaired Student's *t*-test, *$p < 0.05$, **$p < 0.01$; n= 4 independent experiments. **c.** Site-specific detection of m^{6}A on *Hspa1a* 5'UTR-Luc in transfected HeLa cells using fluorescein-dUTP-incorporated primer-extension approach. Both specific (A103) and non-specific (A1280) sites were detected from the same sample. Red boxes highlight decreased probe+1 signals as a result of increased methylation by M3M14-dCas9 but not the inactive mutant. This experiment was repeated twice with similar results. Uncropped scans are shown in Supplementary Fig. 11. **d.** Measurement of m^{6}A levels on endogenous *Hsph1* 5'UTR in MEF cells transfected with engineered m^{6}A

"writers". λ2 sgRNA was used as the non-targeting control. Error bars, mean ± s.e.m.; unpaired Student's *t*-test, *$p < 0.05$; n= 4 independent experiments.

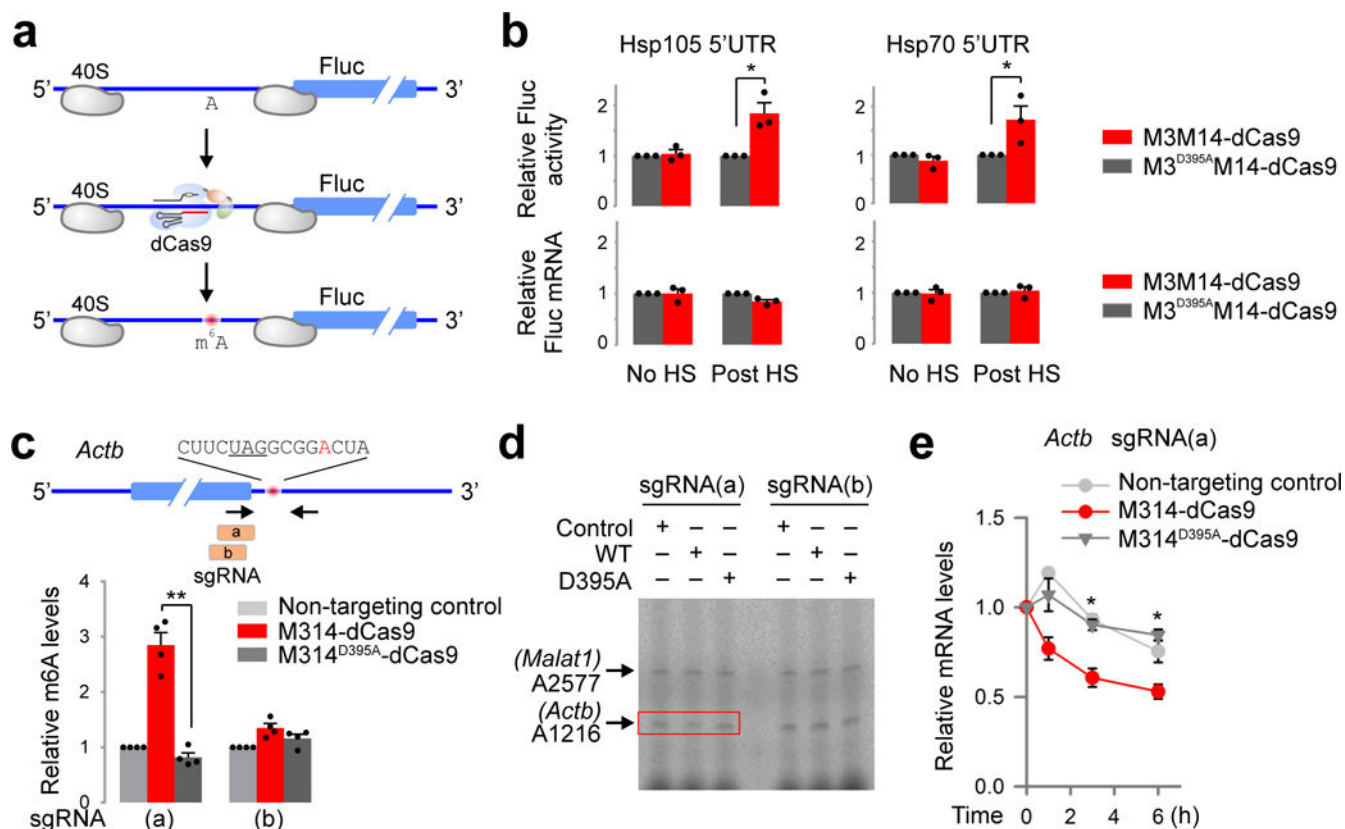**Figure 2 |. Physiological effects of targeted methylation by engineered m^{6}A "writers".**
a. The panel shows possible effects of 5'UTR m^{6}A "writers" on ribosome scanning and subsequent translation. **b.** Translational effects of targeted 5'UTR m^{6}A modification in transfected HeLa cells before and after heat shock (42°C for 1 h). Fluc activities were monitored during heat shock stress recovery. Fluc mRNA levels were also measured in parallel. Error bars, mean ± s.e.m.; unpaired Student's t-test, $*p < 0.05$; n= 3 independent experiments. **c.** Measurement of m^{6}A levels on endogenous *Actb* 3'UTR in HeLa cells transfected with engineered m^{6}A "writers". λ2 sgRNA was used as the non-targeting control. Primers were designed to span the targeting m^{6}A site at A1216 of *Actb* 3'UTR. Error bars, mean ± s.e.m.; unpaired Student's t-test, $**p < 0.01$; n= 4 independent experiments. **d.** Site-specific detection of m^{6}A on endogenous *Actb* in transfected HeLa cells using fluorescein-dUTP-incorporated primer-extension approach. In addition to the specific site (A1216) of *Actb*, the non-specific site (A2577 of *Malat1*) from the same sample was used as negative control. Red boxes highlight decreased probe+1 signals as a result of increased methylation by M3M14-dCas9 but not the inactive mutant. This experiment was repeated three times with similar results. Uncropped scans are shown in Supplementary Fig. 11. **e.** Measurement of *Actb* decay in HeLa cells transfected with engineered m^{6}A "writers". 36 h after transfection, cells were treated with Actinomycin D for various times before sample collection for RT-qPCR. Error bars, mean ± s.e.m.; unpaired Student's t-test, $*p < 0.05$; n= 3 independent experiments.
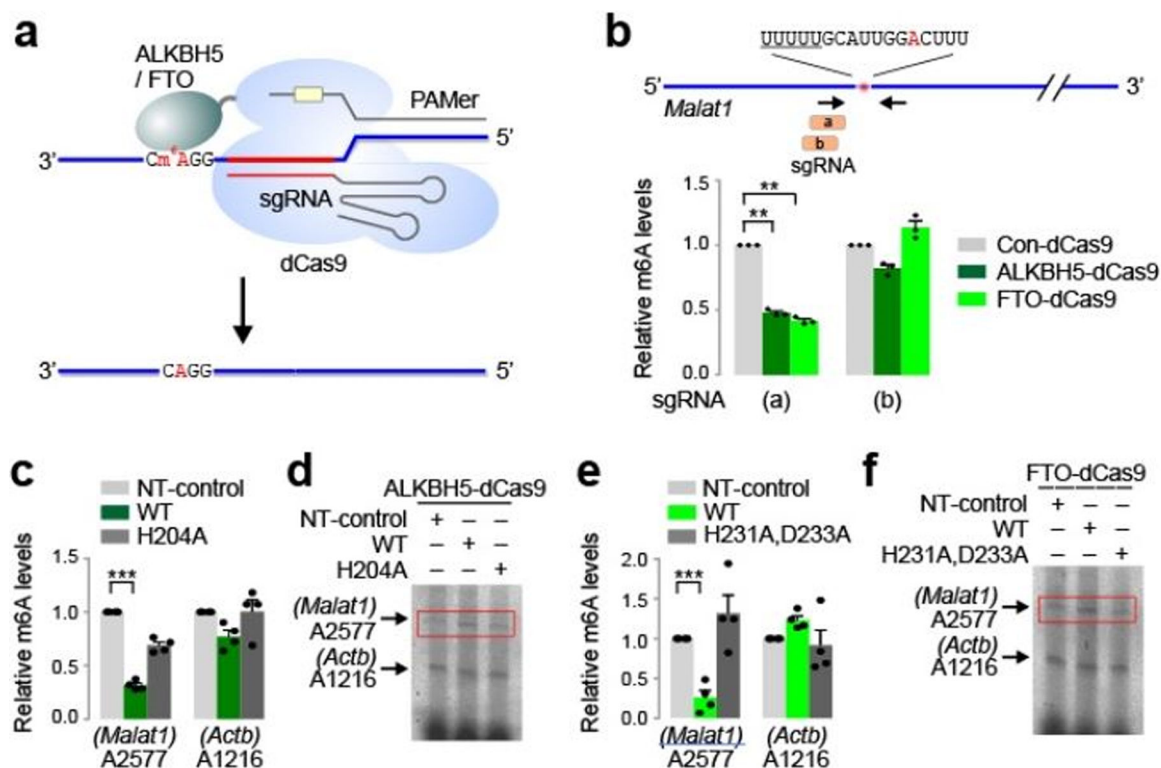
Figure 3 |. Targeted RNA demethylation by engineered m^{6}A "erasers".

a. Schematic of engineered m^{6}A "erasers" by coupling CRISPR-dCas9 with full length ALKBH5 or FTO. The sgRNA and PAMmer are base-paired to nearby regions of the m^{6}A site on target RNA. PAMer supplies the PAM sequence NGG that does not need to be present on target RNA. **b.** Measurement of m^{6}A levels on endogenous *Malat1* in HeLa cells transfected with engineered m^{6}A "erasers". Primers were designed to span the highly methylated m^{6}A site A2577 in *Malat1*. Error bars, mean ± s.e.m.; unpaired Student's t-test, **$p < 0.01$; n= 3 independent experiments. **c.** Measurement of m^{6}A levels on A2577 of *Malat1* and A1216 of *Actb* in HeLa cells transfected with active or inactive ALKBH5-dCas9 in the presence of sgRNA(a). Error bars, mean ± s.e.m.; unpaired Student's t-test, ***$p < 0.001$; n= 4 independent experiments. NT-control indicates non-targeting sgRNA control. **d.** Site-specific detection of m^{6}A using the same samples as **c**. Red boxes highlight increased probe+1 signals as a result of reduced methylation by ALKBH5-dCas9 but not the inactive mutant. NT-control indicates non-targeting sgRNA control. This experiment was repeated twice with similar results. Uncropped scans are shown in Supplementary Fig. 11. **e.** Measurement of m^{6}A levels on A2577 of *Malat1* and A1216 of *Actb* in HeLa cells transfected with active or inactive FTO-dCas9 in the presence of sgRNA(a). Error bars, mean ± s.e.m.; unpaired Student's t-test, ***$p < 0.001$; n= 4 independent experiments. NT-control indicates non-targeting sgRNA control. **f.** Site-specific detection of m^{6}A using the same samples as **e**. Red boxes highlight increased probe+1 signals as a result of reduced methylation by FTO-dCas9 but not the inactive mutant. NT-control indicates non-targeting sgRNA control. This experiment was repeated twice with similar results. Uncropped scans are shown in Supplementary Fig. 11.
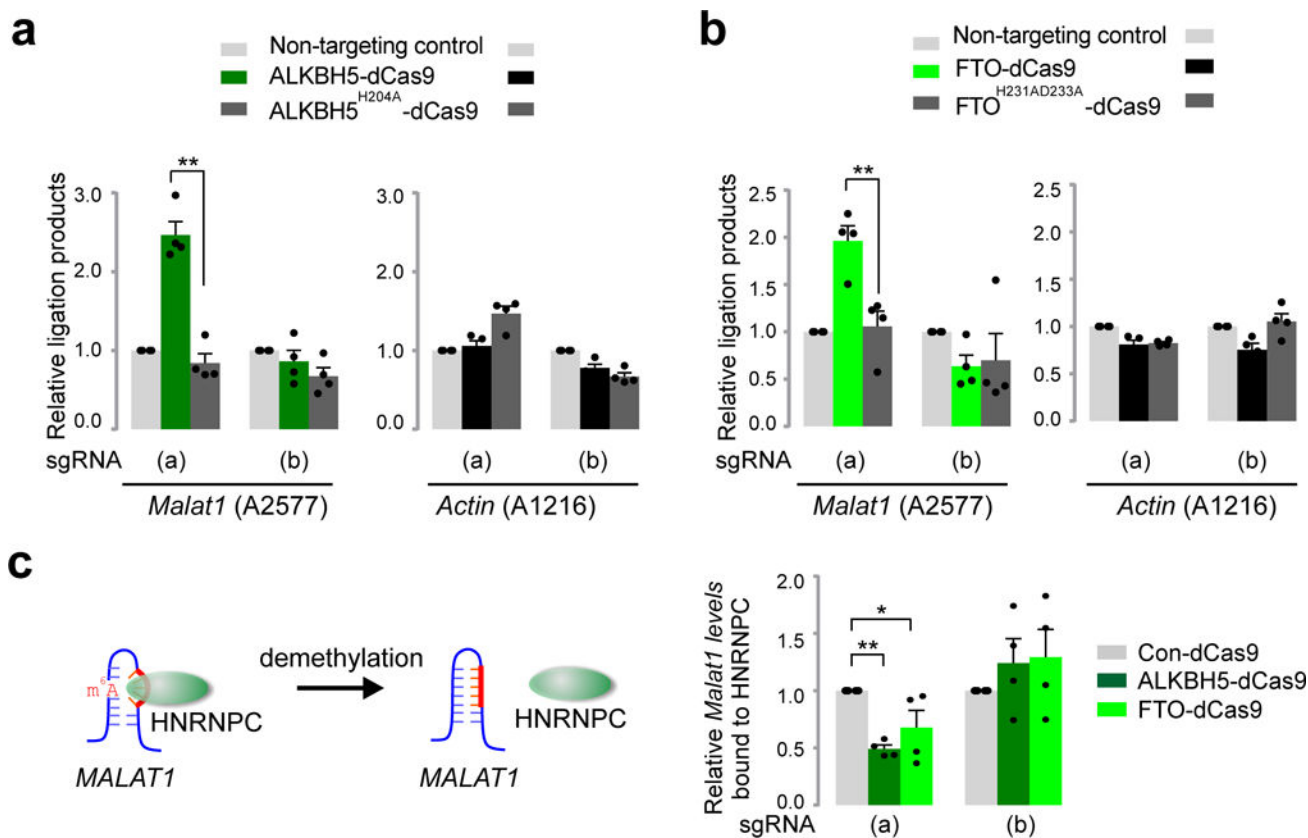
Figure 4 |. Physiological effects of targeted demethylation by engineered m⁶A "erasers".
a. Measurement of m⁶A levels on A2577 of *Malat1* and A1216 of *Actb* in HeLa cells transfected with active or inactive ALKBH5-dCas9 in the presence of sgRNA(a) and sgRNA(b). Error bars, mean ± s.e.m.; unpaired Student's t-test, $**p < 0.01$; n= 4 independent experiments. **b.** Measurement of m⁶A levels on A2577 of Malat1 and A1216 of Actb in HeLa cells transfected with active or inactive FTO-dCas9 in the presence of sgRNA(a) and sgRNA(b). Error bars, mean ± s.e.m.; unpaired Student's t-test, $**p < 0.01$; n= 4 independent experiments. **c.** The left panel depicts the binding of HNRNPC to the U-tract of *Malat1* in the presence of m⁶A. Lack of m⁶A modification leads to HNRNPC dissociation. The right panel shows relative levels of *Malat1* bound to HNRNPC in HeLa cells transfected with engineered m⁶A "erasers". Error bars, mean ± s.e.m.; unpaired Student's t-test, $*p < 0.05$, $**p < 0.01$; n= 4 independent experiments.